The ambiguity-resolved detector
a detector for the mixed-integer GNSS model

Teunissen, P. J.G.

DOI
10.1007/s00190-024-01885-8

Publication date
2024

Document Version
Final published version

Published in
Journal of Geodesy

Journal of Geodesy (2024) 98:83
https://doi.org/10.1007/s00190-024-01885-8

ORIGINAL ARTICLE

The ambiguity-resolved detector: a detector for the mixed-integer GNSS model

P. J. G. Teunissen[1,2,3]

Received: 3 May 2024 / Accepted: 5 August 2024

Abstract
In this contribution, we introduce the ambiguity-resolved (AR) detector and study its distributional characteristics. The AR-detector is a new detector that lies in between the commonly used ambiguity-float (AF) and ambiguity-known (AK) detectors. As the ambiguity vector can seldomly be known completely, usage of the AK-detector is questionable as reliance on its distributional properties will then generally be incorrect. The AR-detector resolves the shortcomings of the AK-detector by treating the ambiguities as unknown integers. We show how the detector improves upon the AF-detector, and we demonstrate that the, for ambiguity-resolved parameter estimation, commonly required extreme success rates can be relaxed for detection, thus showing that improved model validation is also possible with smaller success rates. As such, the AR-detector is designed to work for mixed-integer GNSS models.

Keywords GNSS · Ambiguity-resolved (AR) detector · Ambiguity-float (AF) detector · Ambiguity-known (AK) detector · Integer ambiguity resolution · Detectability · Integer least-squares (ILS)

1 Introduction

Model validation constitutes an essential part of any data processing scheme. This applies to, for instance, quality control of geodetic networks (DGCC 1982; Yang et al. 2021), geophysical and structural deformation analysis (Lehmann and Lösler, 2017; Nowel 2020), different GNSS applications (Perfetti 2006; Yu et al. 2023) and various configurations of integrated navigation systems (Gillissen and Elema 1996; Salzmann 1993). The very first step of model validation is usually the employment of an overall model test to detect for unspecified model misspecifications (Koch 1987; Teunissen 2006). The current detectors in use for mixed-integer GNSS models are the ambiguity-float (AF) and the ambiguity-known (AK) detector (Leick et al. 2015; Teunissen and Montenbruck 2017). The AF-detector considers the ambiguity vector unknown, while the AK-detector assumes the ambiguity vector to be completely known. As the ambiguity vector can seldomly be known completely, the AK-detector is, despite its usage, not really an operational detector. Reliance on its distributional properties will therefore be generally incorrect. The AR-detector of this contribution resolves the shortcomings of the AK-detector by treating the ambiguities as unknown integers. The AR-detector lies therefore in between the AF-detector and the AK-detector. It improves on the AF-detector by incorporating the information that the ambiguities are integer, but it does not consider them known as the AK-detector does. As such, the AR-detector is designed to work for mixed-integer GNSS models.

This contribution is organized as follows. In section 2, after a brief review of mixed-integer model estimation, we describe and compare the ambiguity-float (AF) detector and the ambiguity-known (AK) detector. We also determine their Pythagorean relation and show how their α-acceptance regions are related. What the difference of these regions imply for detectability is discussed. We hereby also introduce a useful orthogonal decomposition of observation space to facilitate the impact description of an arbitrary model bias on the relevant parameters of interest. Then, in section 2.4 the AF- and AK-detection capabilities are explicitly described for a general GNSS model by developing expressions for

✉ P. J. G. Teunissen
p.j.g.teunissen@tudelft.nl

[1] Department of Geoscience and Remote Sensing, Delft University of Technology, Delft, The Netherlands

[2] Department of Infrastructure, University of Melbourne, Melbourne, Australia

[3] GNSS Research Centre, Curtin University of Technology, Perth, Australia

Published online: 12 September 2024

the noncentrality parameters of the detectors. This is done in dependence of four different type of model biases (code-type, phase-type, tropo-type and iono-type). This reveals under which circumstances which model biases find improved detection, thus providing a first indication of the improvements one can expect to gain from the AR-detector.

In section 3, the AR-detector is defined for the admissible class of integer estimators. To enable a direct comparison between the AR- and AK-detector, we show how their CDFs can be seen as differently weighted versions of the CDF of the AF-detector. Special attention is hereby given to the probability mass function of the integer resolved ambiguities. In section 3.3, we describe the different properties of invariance that the detectors exhibit. These properties are instrumental for understanding the performance of the AR-detector in relation to that of the AF- and AK-detector. To evaluate the performance of the AR-detector, we determine its power function and show, by means of the earlier determined orthogonal decomposition, how it is impacted by the different components of a general model bias. For the need of a case-by-case performance evaluation of the AR-detector, we also provide a chi-square calculator-based simulation procedure for computing the detection probabilities in dependence on the assumed model biases. Several examples are provided to illustrate the theory, and the contribution is finalized in section 4 with a summary and conclusions.

The following notation is used throughout. We denote a random variable/vector by means of an underscore; thus, $\underline{x}$ is a random variable/vector, while x is not. $\mathsf{E}(\underline{x})$ and $\mathsf{D}(\underline{x})$ stand for the expectation and dispersion of $\underline{x}$, respectively, $\mathsf{C}(\underline{x}, \underline{y})$ for the covariance between $\underline{x}$ and $\underline{y}$, and $\mathcal{N}_p(\mu, Q)$ denotes a p-dimensional, normally distributed random vector, with mean (expectation) μ and variance matrix (dispersion) Q. $\mathbb{R}^p$ and $\mathbb{Z}^p$ denote the p-dimensional spaces of real and integer numbers, respectively, and the range space of a matrix M is denoted as $\mathcal{R}(M)$. The least-squares (LS) inverse of a full column rank matrix M is denoted as $M^+ = (M^T Q_{yy}^{-1} M)^{-1} M^T Q_{yy}^{-1}$, and the orthogonal projector onto $\mathcal{R}(M)$ as $P_M = MM^+$. $P_M^\perp = I - P_M$ is then the orthogonal projector that projects orthogonally on the orthogonal complement of $\mathcal{R}(M)$. The Q-weighted squared norm is denoted as $||.||_Q^2 = (.)^T Q^{-1}(.)$. $\mathsf{P}[\mathcal{A}]$ denotes the probability of event $\mathcal{A}$, $f_{\underline{x}}(x)$ the probability density function (PDF) of the continuous random vector $\underline{x}$ and $\mathsf{P}[\check{\underline{a}} = z]$ the probability mass function (PMF) of the integer random vector $\check{\underline{a}}$. The noncentral chi-square distribution with p degrees of freedom and noncentrality parameter λ is denoted as $\chi^2(p, \lambda)$ and its α-percentage critical value as $\chi^2_\alpha(p, 0)$.

2 Current GNSS detectors

2.1 The mixed-integer GNSS model

The linear(ized) model of mixed-integer GNSS observation equations is given as,

$$\mathcal{H}_0 : \ \mathsf{E}(\underline{y}) = Aa + Bb \ ; \ a \in \mathbb{Z}^n, b \in \mathbb{R}^p \tag{1}$$

Strang and Borre (1997); Leick et al. (2015); Teunissen and Montenbruck (2017), with the vector of observables $\underline{y} \in \mathbb{R}^m$ containing the carrier-phase and pseudorange data, $[A, B] \in \mathbb{R}^{m \times (n+p)}$ being the given design matrix of full column rank, $a \in \mathbb{Z}^n$ the unknown integer carrier-phase ambiguities, and $b \in \mathbb{R}^p$ the unknown real-valued parameters, such as position coordinates, atmosphere parameters, receiver and satellite clock parameters and instrumental biases. The distribution of the observables is assumed as $\underline{y} \sim \mathcal{N}_m(\mathsf{E}(\underline{y}), Q_{yy})$, with Q_{yy} the given variance matrix of the observed pseudoranges and carrier phases.

The solution to (1) is usually obtained through the following three steps:

Step 1: First the integerness of the ambiguities is discarded. Application of the Q_{yy}-weighted least-squares (LS) principle provides then the solution, together with its vc-matrix, as

$$\begin{bmatrix} \hat{\underline{a}} \\ \hat{\underline{b}} \end{bmatrix} = \begin{bmatrix} \bar{A}^+ \underline{y} \\ \bar{B}^+ \underline{y} \end{bmatrix} \ , \ \begin{bmatrix} Q_{\hat{a}\hat{a}} & Q_{\hat{a}\hat{b}} \\ Q_{\hat{b}\hat{a}} & Q_{\hat{b}\hat{b}} \end{bmatrix} \tag{2}$$

with $\bar{A} = P_B^\perp A$ and $\bar{B} = P_A^\perp B$. This solution is referred to as the ambiguity *float* solution.

Step 2: Then, an admissible integer map $\mathcal{I} : \mathbb{R}^n \mapsto \mathbb{Z}^n$ is chosen to compute the integer ambiguity vector as

$$\check{\underline{a}} = \mathcal{I}(\hat{\underline{a}}) \tag{3}$$

The integer map is admissible when its *pull-in regions* $\mathcal{P}_z = \{x \in \mathbb{R}^n | \ \mathcal{I}(x) = z\}$, $z \in \mathbb{Z}^n$, cover $\mathbb{R}^n$, while being disjoint and integer translational invariant (Teunissen 2000). Some popular choices for $\mathcal{I}$ are integer rounding (IR), integer bootstrapping (IB), or integer least-squares (ILS). Teunissen (1999a) has shown that these estimators can be ordered in terms of their ambiguity success rates (i.e. probability of correct integer estimation) as

$$\mathsf{P}[\check{\underline{a}}_{\mathrm{IR}} = a] \leq \mathsf{P}[\check{\underline{a}}_{\mathrm{IB}} = a] \leq \mathsf{P}[\check{\underline{a}}_{\mathrm{ILS}} = a] \tag{4}$$

Step 3: Once the integer ambiguity solution is obtained, the float baseline solution of the first step is corrected, so as to obtain the ambiguity-resolved baseline solution as

$$\check{\underline{b}} = \hat{\underline{b}} - Q_{\hat{b}\hat{a}} Q_{\hat{a}\hat{a}}^{-1} (\hat{\underline{a}} - \check{\underline{a}}) \tag{5}$$

This solution is referred to as the ambiguity *fixed* baseline solution. To obtain a precise fixed baseline solution, one needs to resolve the ambiguities with a very high success rate. When the success rate is high enough, one may neglect the uncertainty in $\check{\underline{a}}$ and describe the uncertainty in $\check{\underline{b}}$ by means of the PDF of $\hat{\underline{b}}(a)$. This is made precise by the following bounds of Teunissen (1999b),

$$\mathsf{P}[\hat{\underline{b}}(a) \in \Omega]\mathsf{P}[\check{\underline{a}} = a] \leq \mathsf{P}[\check{\underline{b}} \in \Omega] \leq \mathsf{P}[\hat{\underline{b}}(a) \in \Omega]$$

which hold true for any convex region $\Omega \subset \mathbb{R}^p$ centred at $\mathsf{E}(\hat{\underline{b}})$. Thus, when the success rate is close enough to 1, then $\mathsf{P}[\check{\underline{b}} \in \Omega] \approx \mathsf{P}[\hat{\underline{b}}(a) \in \Omega]$, which in case of GNSS, due to the very precise carrier-phase data, is usually a much larger probability than that obtained from the float-solution $\hat{\underline{b}}$, $\mathsf{P}[\hat{\underline{b}}(a) \in \Omega] \gg \mathsf{P}[\hat{\underline{b}} \in \Omega]$. Thus, very high ambiguity success rates are needed in order to achieve precise baseline estimation, i.e.

$$\mathsf{P}[\check{\underline{b}} \in \Omega] \gg \mathsf{P}[\hat{\underline{b}} \in \Omega] \tag{6}$$

In this contribution, we will show, however, that this is not necessarily so if one wants to exploit the integerness of the ambiguities for model validation.

Although we will be working in the following with the *batch* formulation (1), we remark that the presented theory applies equally well to the validation of models underlying *recursive* estimation, such as recursive least-squares estimation and/or Kalman filtering, see, for example, Teunissen and Salzmann (1989); Teunissen and Montenbruck (2017). Hence, in analogy with ambiguity resolution-based Kalman filtering, the ambiguity-resolved detector can also be used in real-time applications.

2.2 The AF and AK detector

The two detectors that are commonly used for the detection of model misspecifications in (1) are the ambiguity-float (AF) detector and the ambiguity-known (AK) detector. They are based on assuming the integer ambiguity vector to be either an unknown real-valued vector or a given known vector. They are defined as follows.

Definition 1 (AF- and AK-detectors) With the distribution of the Q_{yy}-weighted squared norms of the two least-squares residual vectors, $\hat{\underline{e}} = P_{[A,B]}^{\perp} \underline{y}$ and $\hat{\underline{e}}(a) = P_B^{\perp}(\underline{y} - Aa)$, given under the null hypothesis (1) as

$$\begin{aligned} ||\hat{\underline{e}}||_{Q_{yy}}^2 &\overset{\mathcal{H}_0}{\sim} \chi^2(r, 0), \ r = m - (n + p) \\ ||\hat{\underline{e}}(a)||_{Q_{yy}}^2 &\overset{\mathcal{H}_0}{\sim} \chi^2(r(a), 0), \ r(a) = m - p \end{aligned} \tag{7}$$

the two detector tests read:

$$\begin{aligned} &\text{AF} : \text{Accept } \mathcal{H}_0 \text{ if } ||\hat{\underline{e}}||_{Q_{yy}}^2 \leq \chi_\alpha^2(r, 0) \\ &\text{AK} : \text{Accept } \mathcal{H}_0 \text{ if } ||\hat{\underline{e}}(a)||_{Q_{yy}}^2 \leq \chi_\alpha^2(r(a), 0) \end{aligned} \tag{8}$$

or reject the null hypothesis otherwise. ■

In order to compare the two detectors, we first establish their relationship by means of the geometry of orthogonal projectors. As $P_{[A,B]} = P_{\bar{A}} + P_B$, with $\bar{A} = P_B^{\perp} A$, we have

$$P_B^{\perp} = P_{[A,B]}^{\perp} + P_{\bar{A}} \tag{9}$$

from which the relation between the two residual vectors follows as $\hat{\underline{e}}(a) = \hat{\underline{e}} + P_{\bar{A}}(\underline{y} - Aa)$, giving for their Q_{yy}-weighted squared norms, the decomposition $||\hat{\underline{e}}(a)||_{Q_{yy}}^2 = ||\hat{\underline{e}}||_{Q_{yy}}^2 + ||P_{\bar{A}}(\underline{y} - Aa)||_{Q_{yy}}^2$. The last term of this decomposition can be further expressed in the *ambiguity residual* $\hat{\underline{\epsilon}}(a) = \hat{\underline{a}} - a$ as $||P_{\bar{A}}(\underline{y} - Aa)||_{Q_{yy}}^2 = ||\hat{\underline{a}} - a||_{Q_{\hat{a}\hat{a}}}^2$. This follows from using $P_{\bar{A}} = \bar{A}\bar{A}^+$, $\bar{A}^+ \underline{y} = \hat{\underline{a}}$ and $Q_{\hat{a}\hat{a}} = (\bar{A}^T Q_{yy}^{-1} \bar{A})^{-1}$. Hence, this establishes the following relation between the two detectors.

Lemma 1 *(AK-AF Pythagorean relation) The AF- and AK-detectors are linked through the Pythagorean relation*

$$||\hat{\underline{e}}(a)||_{Q_{yy}}^2 = ||\hat{\underline{e}}||_{Q_{yy}}^2 + ||\hat{\underline{\epsilon}}(a)||_{Q_{\hat{a}\hat{a}}}^2 \tag{10}$$

in which $||\hat{\underline{\epsilon}}(a)||_{Q_{\hat{a}\hat{a}}}^2 = ||\hat{\underline{a}} - a||_{Q_{\hat{a}\hat{a}}}^2$. ■

Another important property that follows from the orthogonality $\hat{\underline{e}}^T Q_{yy}^{-1} \bar{A} = 0$ is that the two terms on the right-hand side of (10) are independent. The relation (10) is very useful for comparing the two detectors and for visualizing the relationship between their respective acceptance regions. The acceptance regions of the two detector tests are given as

$$\begin{aligned} \mathcal{A}_{\text{AF}} &= \{x \in \mathbb{R}_0^+ | x = ||\hat{e}||_{Q_{yy}}^2 \leq \chi_\alpha^2(r, 0)\} \\ \mathcal{A}_{\text{AK}} &= \{z \in \mathbb{R}_0^+ | z = ||\hat{e}(a)||_{Q_{yy}}^2 \leq \chi_\alpha^2(r(a), 0)\} \end{aligned} \tag{11}$$

For the purpose of a geometric comparison, the acceptance regions of the AF-detector and the AK-detector are shown in a two-dimensional fashion in Fig. 1. Note, in order for the two detectors to have the same false-alarm probabilities, the critical value of the AK-detector has to be larger than that of

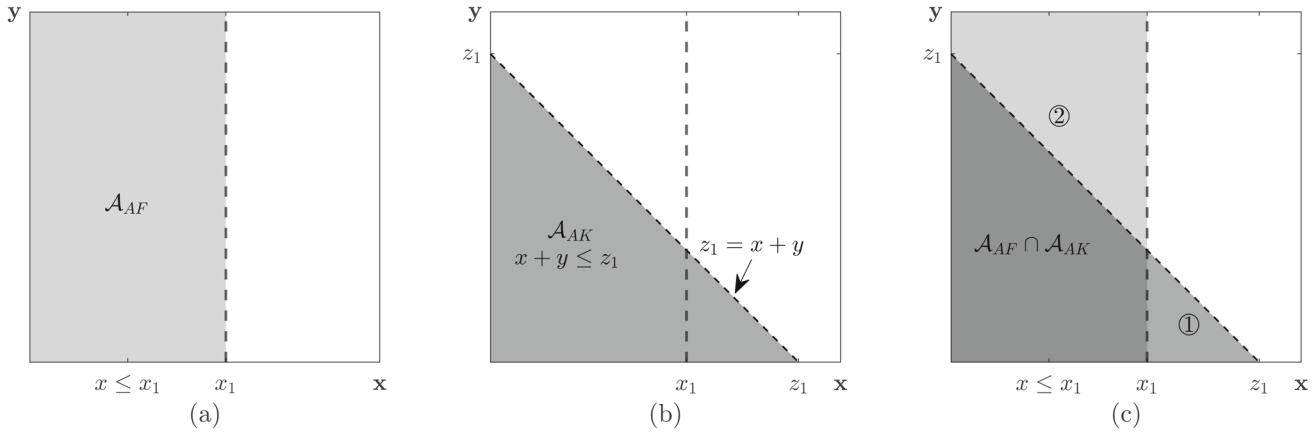

Fig. 1 AF- and AK-acceptance regions: (a) $\mathcal{A}_{\text{AF}} = \{x, y \in \mathbb{R}_0^+ | \; x = ||\hat{e}||^2_{Q_{yy}} \leq x_1 = \chi^2_\alpha(r, 0)\}$; (b) $\mathcal{A}_{\text{AK}} = \{x, y \in \mathbb{R}_0^+ | \; z = ||\hat{e}(a)||^2_{Q_{yy}} = x + y \leq z_1 = \chi^2_\alpha(r(a), 0)\}$, with $x = ||\hat{e}||^2_{Q_{yy}}$, $y = ||\hat{\epsilon}(a)||^2_{Q_{\hat{a}\hat{a}}}$; and (c) difference of $\mathcal{A}_{\text{AF}}$ and $\mathcal{A}_{\text{AK}}$

the AF-detector, $\chi^2_\alpha(r(a), 0) > \chi^2_\alpha(r, 0)$. Would this not be the case, the AK-acceptance region would become a subset of the AF-acceptance region, $\mathcal{A}_{\text{AK}} \subset \mathcal{A}_{\text{AF}}$, and thus always have a smaller false-alarm probability.

When we compare $\mathcal{A}_{\text{AK}}$ with $\mathcal{A}_{\text{AF}}$, we note that $\mathcal{A}_{\text{AK}}$ has a *surplus*-region when $\chi^2_\alpha(r, 0) \leq ||\hat{e}||^2_{Q_{yy}} \leq \chi^2_\alpha(r(a), 0)$ (indicated as ① in Fig. 1c) and a *deficit*-region when $||\hat{e}||^2_{Q_{yy}} \leq \chi^2_\alpha(r, 0)$ (indicated as ② in Fig. 1c). The consequence of the surplus-region ① is that for small $y = ||\hat{\epsilon}(a)||^2_{Q_{\hat{a}\hat{a}}}$, larger values of $||\hat{e}||^2_{Q_{yy}}$ will be accepted with the AK-detector than otherwise would be the case with AF-detector. Modelling errors that hardly affect $||\hat{\epsilon}(a)||^2_{Q_{\hat{a}\hat{a}}}$ will therefore be rejected less often by the AK-detector than by the AF-detector. The consequence of the deficit-region ②, on the other hand, is that it eliminates the lack of sensitivity of the AF-detector for modelling errors affecting $y = ||\hat{\epsilon}(a)||^2_{Q_{\hat{a}\hat{a}}}$. Hence, one could say that the presence of ① is the price the AK-detector has to pay for being sensitive for ②.

2.3 Comparing AF and AK detectability

In order to be able to compare the performance of the AF-detector with the AK-detector further, the following general alternative hypothesis is used,

$$\mathcal{H}_a : \; \mathsf{E}(\underline{y}) = Aa + Bb + Cc \; ; \; c \in \mathbb{R}^q \tag{12}$$

whereby matrix $[A, B, C] \in \mathbb{R}^{m \times (n+p+q)}$ is assumed to be of full column rank. Thus, under $\mathcal{H}_a$, the mean of $\underline{y}$ is assumed shifted by Cc, $\mathsf{E}(\underline{y}|\mathcal{H}_a) = \mathsf{E}(\underline{y}|\mathcal{H}_0) + Cc$. Such shifts allow us to model various important GNSS model misspecifications. For instance, through the choice of C in Cc one may model the presence of one or more outliers in the pseudorange data, or cycle slips in the phase data, or the presence of neglected atmospheric effects, or in fact any other systematic effect that one failed to take into account under the null hypothesis $\mathcal{H}_0$ (cf. 1).

Under the alternative hypothesis (12), the two detectors and their difference are noncentral chi-square distributed as

$$\begin{aligned} ||\underline{\hat{e}}||^2_{Q_{yy}} &\overset{\mathcal{H}_a}{\sim} \chi^2(r, \lambda_{\hat{e}}) \\ ||\underline{\hat{e}}(a)||^2_{Q_{yy}} &\overset{\mathcal{H}_a}{\sim} \chi^2(r(a), \lambda_{\hat{e}(a)}) \\ ||\underline{\hat{\epsilon}}(a)||^2_{Q_{\hat{a}\hat{a}}} &\overset{\mathcal{H}_a}{\sim} \chi^2(n, \lambda_{\hat{\epsilon}(a)}) \end{aligned} \tag{13}$$

with noncentrality parameters

$$\begin{aligned} \lambda_{\hat{e}} &= ||P^\perp_{[A,B]} Cc||^2_{Q_{yy}} \\ \lambda_{\hat{e}(a)} &= ||P^\perp_B Cc||^2_{Q_{yy}} \\ \lambda_{\hat{\epsilon}(a)} &= ||P_{\bar{A}} Cc||^2_{Q_{yy}} \end{aligned} \tag{14}$$

These distributional results can now be used to determine the power functions or detection probabilities of the two detectors. We have

$$\begin{aligned} \mathsf{P}[||\underline{\hat{e}}||^2_{Q_{yy}} > \chi^2_\alpha(r, 0)|\mathcal{H}_a] &= \gamma_{\text{AF}} \\ \mathsf{P}[||\underline{\hat{e}}(a)||^2_{Q_{yy}} > \chi^2_\alpha(r(a), 0)|\mathcal{H}_a] &= \gamma_{\text{AK}} \end{aligned} \tag{15}$$

They depend on the user-chosen false-alarm rate α, the model redundancy, r or $r(a)$, and through the noncentrality parameter, $\lambda_{\hat{e}}$ or $\lambda_{\hat{e}(a)}$, on the bias vector Cc. For the redundancies (degrees of freedom) and noncentrality parameters of the two detectors, we have the relations

$$r(a) = r + n \;\; \text{and} \;\; \lambda_{\hat{e}(a)} = \lambda_{\hat{e}} + \lambda_{\hat{\epsilon}(a)} \tag{16}$$

where the second expression follows from applying (9) to (14). The AK-detector will have a larger power than the AF-detector if $\gamma_{\text{AK}} > \gamma_{\text{AF}}$. Such is, however, not guaranteed

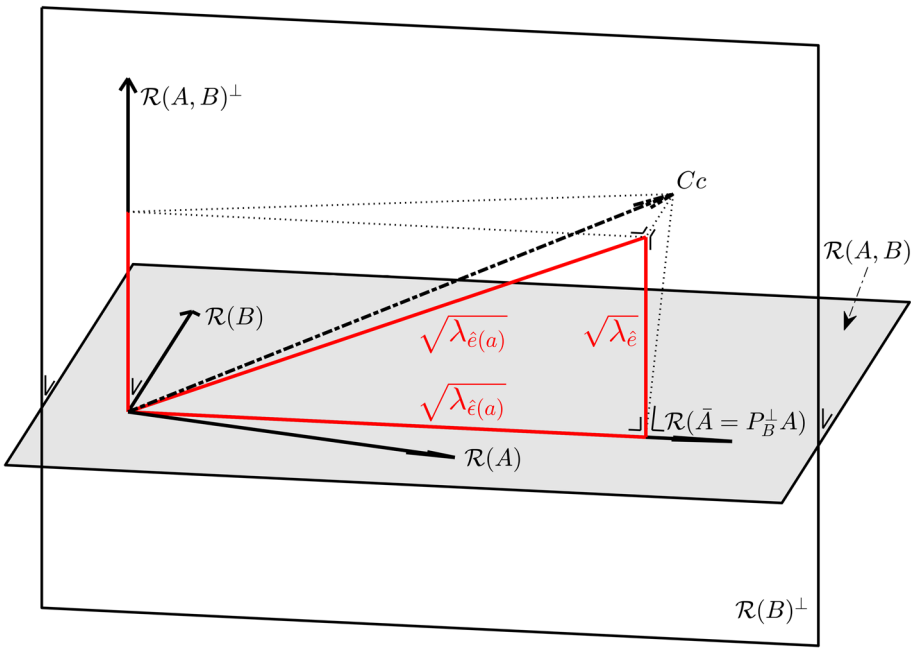

Fig. 2 The orthogonal decomposition $\mathbb{R}^m = \mathcal{R}(\bar{A}) \oplus \mathcal{R}(B) \oplus \mathcal{R}(A,B)^{\perp}$, with projections $P_{\bar{A}}Cc$ and $P_B^{\perp}Cc$, giving $\lambda_{\hat{e}(a)} = ||P_{\bar{A}}Cc||^2_{Q_{yy}}$ and $\lambda_{\hat{e}(a)} = ||P_B^{\perp}Cc||^2_{Q_{yy}}$, where $\lambda_{\hat{e}} = \lambda_{\hat{e}(a)} - \lambda_{\hat{\epsilon}(a)} = ||P^{\perp}_{[A,B]}Cc||^2_{Q_{yy}}$

in general, since the AK-detector has not only a larger non-centrality parameter, but also larger degrees of freedom. The increase in degrees of freedom increases the variability of $||\underline{\hat{e}}(a)||^2_{Q_{yy}}$, thus requiring a larger critical value for the same false-alarm probability, i.e. $\chi^2_{\alpha}(r(a),0) > \chi^2_{\alpha}(r,0)$, since $r(a) > r$, see also Fig. 1. This larger critical value reduces the rejection region and therefore goes at the expense of an increase in power. It is therefore the balance that is stricken between the increase in critical value and the increase in non-centrality parameter that determines whether or not the power increases for the particular alternative hypothesis considered. For instance, knowing the ambiguity vector a will not help to increase the power if $\lambda_{\hat{e}} = \lambda_{\hat{e}(a)}$, while it certainly will increase the power when $\lambda_{\hat{e}} = 0$ and $\lambda_{\hat{e}(a)} \neq 0$. This latter case suggests that the power will also increase if $\lambda_{\hat{e}}$ is small and $\lambda_{\hat{e}(a)}$ sufficiently large.

To be more specific, we need to know how matrix C of $\mathcal{H}_a$ (cf. 12) propagates through the projectors present in the non-centrality parameters of (14). In order to do so, we specify the components of C with respect to an *orthogonal decomposition* of observation space $\mathbb{R}^m$. The three subspaces that make up this orthogonal decomposition are $\mathcal{R}(\bar{A})$, $\mathcal{R}(B)$ and $\mathcal{R}(A,B)^{\perp}$. It is not difficult to verify that they are mutually orthogonal and together form a direct sum of observation space, $\mathbb{R}^m = \mathcal{R}(\bar{A}) \oplus \mathcal{R}(B) \oplus \mathcal{R}(A,B)^{\perp}$, see Fig. 2. From the geometry of the figure, conclusions about the following extreme cases can be directly made:

Improved detectability The AF-detector will have zero detectability if $\lambda_{\hat{e}} = 0$ ($\mathcal{R}(C) \subset \mathcal{R}(A,B) = \mathcal{R}(\bar{A},B)$) and the AK-detector a nonzero detectability if $\lambda_{\hat{e}(a)} \neq 0$ ($\mathcal{R}(C) \not\subset \mathcal{R}(B)$). These conditions are satisfied iff matrix C is expressible as $C = [A,B][X^T, Y^T]^T$ for some matrices $X \neq 0$ and Y.

No improved detectability The AK-detector will not have an improvement if $\lambda_{\hat{e}} = \lambda_{\hat{e}(a)}$, i.e. if $\lambda_{\hat{\epsilon}(a)} = 0$ ($\mathcal{R}(C) \subset \mathcal{R}(\bar{A})^{\perp}$). This happens when matrix C is expressible as $C = [B,[A,B]^{\perp}][X^T, Y^T]^T$ for some matrices X and Y, whereby $[A,B]^{\perp}$ is a basis matrix of $\mathcal{R}(A,B)^{\perp}$. If $Y = 0$, then $\lambda_{\hat{e}} = \lambda_{\hat{e}(a)} = 0$.

2.4 The single-epoch GNSS model

To exemplify the detectability of the two detectors, we consider the single-epoch, f-frequency, geometry-based m double-differenced (DD) pseudorange, and carrier-phase GNSS model under a general alternative hypothesis, see, for example, Teunissen and Montenbruck (2017),

$$\mathcal{H}_a : \mathsf{E}\begin{bmatrix}\underline{p}\\ \underline{\phi}\end{bmatrix} = \underbrace{\begin{bmatrix}0 & G & C_p\\ L & G & C_\phi\end{bmatrix}}_{\begin{matrix}\uparrow & \uparrow & \uparrow\\ A & B & C\end{matrix}}\begin{bmatrix}a\\ b\\ c\end{bmatrix}, \tag{17}$$

with $\mathsf{D}(\underline{p}) = Q_{pp} = \sigma_p^2 Q$, $\mathsf{D}(\underline{\phi}) = Q_{\phi\phi} = \sigma_\phi^2 Q$ and $\mathsf{C}(\underline{p},\underline{\phi}) = 0$. In (17), the pseudorange and carrier-phase data are collected in $\underline{p},\underline{\phi} \in \mathbb{R}^{fm}$, the fm integer DD ambiguities in $a \in \mathbb{Z}^{fm}$, the real-valued GNSS parameters, like baseline components and possibly atmospheric delays, in $b \in \mathbb{R}^p$, and the hypothesized q model biases in $c \in \mathbb{R}^q$. The design matrices in (17) are: $L = \Lambda \otimes I_m \in \mathbb{R}^{fm\times fm}$, with $\Lambda = \mathrm{diag}(\lambda_1,\ldots,\lambda_f)$ and λ_i the wavelength of the ith frequency; $G = e_f \otimes \mathcal{G} \in \mathbb{R}^{fm\times p}$, with e_f the f-vector

of ones and $\mathcal{G} \in \mathbb{R}^{m\times p}$ the DD receiver-satellite geometry matrix; and $C_p, C_\phi \in \mathbb{R}^{fm\times q}$ the signature matrices that link the hypothesized model bias with the observables.

To be able to compare the detectability of the AF- and AK-detector for the above GNSS model, we need to work out the expressions for their noncentrality parameters.

Lemma 2 *(AF-AK noncentrality) For the single-epoch GNSS model (17), the noncentrality parameters of the AF- and AK-detectors are given as*

$$\begin{aligned}\lambda_{\hat{e}} &= ||P_G^\perp C_p c||^2_{Q_{pp}}\\ \lambda_{\hat{e}(a)} &= \lambda_{\hat{e}} + ||P_G^\perp C_\phi c||^2_{Q_{\phi\phi}} + \frac{||P_G(C_p - C_\phi)c||^2_{Q_{pp}}}{1+\sigma_\phi^2/\sigma_p^2}\end{aligned} \tag{18}$$

with projectors $P_G = G(G^T Q_{pp}^{-1} G)^{-1} G^T Q_{pp}^{-1}$ and $P_G^\perp = I - P_G$.

Proof See Appendix. □

The structure of (18) can be understood as follows. As matrix L of (17) is invertible, the phase data will not contribute to any detectability in case the ambiguities are unknown. This explains why the above $\lambda_{\hat{e}}$ does not depend on C_ϕ. For the case the ambiguities are known, the phase data act as if they are pseudorange data, resulting in a second term of $\lambda_{\hat{e}(a)}$ that has a form similar to that of $\lambda_{\hat{e}}$. The first two terms of the above $\lambda_{\hat{e}(a)}$ describe therefore the detectability contributions of the pseudorange and phase data for the case their baselines would be uncoupled. But as their baselines are the same, an additional detectability enters, which is described by the last term of the above $\lambda_{\hat{e}(a)}$.

Note, when matrix G is invertible that (18) simplifies considerably. Then, $P_G = I$ and $P_G^\perp = 0$, thus giving

$$\begin{aligned}\lambda_{\hat{e}} &= 0\\ \lambda_{\hat{e}(a)} &= \frac{||(C_p - C_\phi)c||^2_{Q_{pp}}}{1+\sigma_\phi^2/\sigma_p^2}\end{aligned} \tag{19}$$

Hence, detection with the AF-detector is then impossible and detection with the AK-detector is only possible for $C_p \neq C_\phi$. The case of matrix G being invertible happens in the single-frequency case, when $\mathcal{G}$ is invertible, i.e. $m = p$.

For when G is not invertible, we now consider four different types of model biases and work out the expressions for their noncentrality parameters. The four types considered are: code-type ($C_\phi = 0$), phase-type ($C_p = 0$), tropo-type ($C_p = C_\phi$) and iono-type ($C_p = -C_\phi$):

Code-type ($C_\phi = 0$): These are any model biases that only affect the pseudoranges. They could, for instance, be a single outlier in one of the DD pseudoranges, in which case $q = 1$ and C_p is a canonical unit vector having its 1 at the slot of the suspected DD pseudorange, or multiple pseudorange outliers, for instance, in the ith DD pseudorange of all f signals, in which case $q = f$ and $C_p = I_f \otimes c_i$, with c_i the ith canonical unit vector. With $C_\phi = 0$, expressions (18) specialize to

$$\begin{aligned}\lambda_{\hat{e}} &= ||P_G^\perp C_p c||^2_{Q_{pp}}\\ \lambda_{\hat{e}(a)} &= \lambda_{\hat{e}} + \frac{||P_G C_p c||^2_{Q_{pp}}}{1+\sigma_\phi^2/\sigma_p^2} \approx ||C_p c||^2_{Q_{pp}}\end{aligned} \tag{20}$$

The last approximation follows from using the matrix identity $I_m = P_G + P_G^\perp$ and the GNSS-admitted assumption that the carrier-phase observables are much more precise than the pseudorange observables ($\sigma_\phi^2 \ll \sigma_p^2$). As a result we see that both noncentrality parameters of (20) are driven by the pseudorange precision σ_p^2 and that $\lambda_{\hat{e}(a)}$ has become independent of the receiver-satellite geometry matrix G. Hence, in contrast to the AF-detector, the AK-detector will be able to detect model biases for which $\mathcal{R}(C_p) \subset \mathcal{R}(G)$.

An example of the significant impact that knowing the ambiguity vector has on testing is shown in Fig. 3 for a single-epoch, single-frequency GNSS model. The poor performance of the pseudorange driven AF-detector is due to the fact that all receiver-satellite direction vectors, except that of

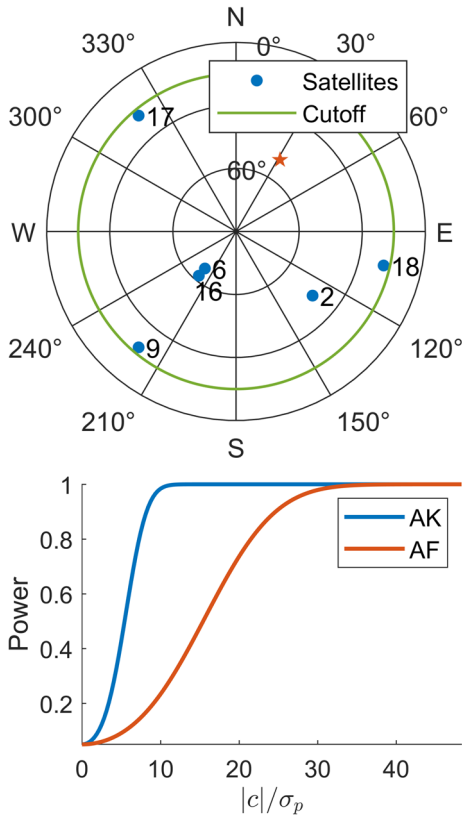

Fig. 3 (Top) GPS skyplot with PRNs 2, 6, 9, 16, 17, 18. The star indicates the symmetry axis of the cone determined by all PRNs excluding PRN 9; after (Teunissen and Montenbruck (2017)), page 700; (Bottom) AF- and AK-powercurves for outlier in PRN 9, with $\alpha = 0.05$ and $\sigma_\phi = \sigma_p/100$

PRN 9, approximately lie on a common cone, the symmetry axis of which is indicated with a star in the skyplot. This is further explained in Teunissen and Montenbruck (2017), page 700.

Phase-type ($C_p = 0$): These are any model biases that only affect the carrier phases. They could, for instance, be single or multiple cycle slips in the phase data, unmodelled instrumental phase delays, or, in case of PPP-RTK, outliers in the provided phase-biases (Duan et al. 2024). With $C_p = 0$, expressions (18) specialize to

$$\begin{aligned}\lambda_{\hat{e}} &= 0\\ \lambda_{\hat{e}(a)} &= \lambda_{\hat{e}} + ||P_G^{\perp} C_\phi c||^2_{Q_{\phi\phi}} + \frac{||P_G C_\phi c||^2_{Q_{pp}}}{1+\sigma_\phi^2/\sigma_p^2}\\ &\approx \begin{cases} ||C_\phi c||^2_{Q_{pp}} \text{ if } \mathcal{R}(C_\phi) \subset \mathcal{R}(G)\\ ||P_G^{\perp} C_\phi c||^2_{Q_{\phi\phi}} \text{ otherwise}\end{cases}\end{aligned} \tag{21}$$

That $\lambda_{\hat{e}} = 0$ follows of course from the fact that, in the single-epoch case, the carrier-phase observation equations have, through their unknown ambiguities, as many unlinked parameters as equations. Hence, the presence of any additional unlinked parameters, such as those of the phase model biases, will remain undetected. This situation changes in case the ambiguities are known. The detectability will then generally be driven by the very precise carrier-phase data, unless $\mathcal{R}(C_\phi) \subset \mathcal{R}(G)$, in which case it is driven by the poorer pseudorange precision. The conclusion reads therefore that for phase-type model biases, knowledge of the ambiguities turns the AF-undetectability in a very strong AK detectability.

Tropo-type ($C_p = C_\phi = C_\tau$): These are any model biases that affect the pseudoranges and the carrier phases in an identical way. If assumed absent under $\mathcal{H}_0$, these could, for instance, be the tropospheric delays. Would one model the wet zenith tropospheric delay by means of mapping functions, then $q = 1$ and $C_\tau = e_f \otimes c_\tau$, with c_τ being the m-vector of differenced mapping functions and e_f the f-vector of ones. Would one include horizontal tropospheric gradients as well, then $q = 3$ and c_τ becomes an $m \times 3$ matrix. With $C_p = C_\phi = C_\tau$, expressions (18) specialize to

$$\begin{aligned}\lambda_{\hat{e}} &= ||P_G^{\perp} C_\tau c||^2_{Q_{pp}}\\ \lambda_{\hat{e}(a)} &= \lambda_{\hat{e}} + ||P_G^{\perp} C_\tau c||^2_{Q_{\phi\phi}}\\ &= \begin{cases} 0 \text{ if } \mathcal{R}(C_\tau) \subset \mathcal{R}(G)\\ \approx ||P_G^{\perp} C_\tau c||^2_{Q_{\phi\phi}} \text{ otherwise}\end{cases}\end{aligned} \tag{22}$$

This shows that we generally see an improvement by a large factor σ_p^2/σ_ϕ^2 when changing from the AF-detector to the AK-detector. This improvement is only absent when $\mathcal{R}(C_\tau) \subset \mathcal{R}(G)$, in which case both noncentrality parameters are equal to zero, $\lambda_{\hat{e}} = \lambda_{\hat{e}(a)} = 0$. However, note that tropo-type biases will never be detectable, i.e. not by the AF-detector and not by the AK-detector, in case G is invertible (cf. 19).

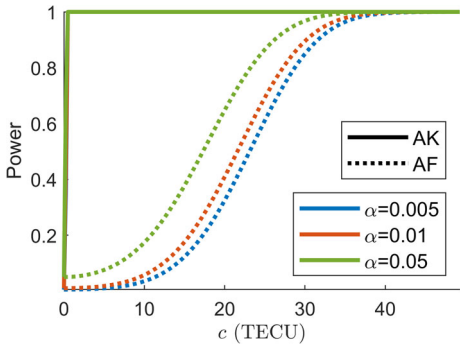

Fig. 4 AK- and AF-power function curves for ionosphere detection as function of iono-delay in TEC units, for different false-alarm probabilities (levels of significance α), based on a single-epoch, dual-frequency L1/L5 GPS model, with $\sigma_p = 50$cm and $\sigma_\phi = 5$mm

Iono-type ($C_p = -C_\phi = C_\iota$): These are any model biases that affect the pseudoranges and the carrier phases in the same, but oppositely signed, way. If assumed absent under $\mathcal{H}_0$, these could, for instance, be the ionospheric delays. With $C_p = -C_\phi = C_\iota$, expressions (18) specialize to

$$\begin{aligned}\lambda_{\hat{e}} &= ||P_G^{\perp} C_\iota c||^2_{Q_{pp}}\\ \lambda_{\hat{e}(a)} &= \lambda_{\hat{e}} + ||P_G^{\perp} C_\iota c||^2_{Q_{\phi\phi}} + \frac{4||P_G C_\iota c||^2_{Q_{pp}}}{1+\sigma_\phi^2/\sigma_p^2}\\ &\approx \begin{cases} 4||C_\iota c||^2_{Q_{pp}} \text{ if } \mathcal{R}(C_\iota) \subset \mathcal{R}(G)\\ ||P_G^{\perp} C_\iota c||^2_{Q_{\phi\phi}} \text{ otherwise}\end{cases}\end{aligned} \tag{23}$$

As with the tropo-type biases, we see again an improvement by the large factor σ_p^2/σ_ϕ^2 when changing from the AF-detector to the AK-detector. Different from the tropo-type case is, however, that the AK-detector now still has, in contrast to the AF-detector, detectability when $\mathcal{R}(C_\iota) \subset \mathcal{R}(G)$. Also, note that for $C_\tau = C_\iota$, $\lambda_{\hat{e}(a)}(\text{iono}) - \lambda_{\hat{e}(a)}(\text{tropo}) = \frac{4||P_G C_\tau c||^2_{Q_{pp}}}{1+\sigma_\phi^2/\sigma_p^2} \geq 0$.

To illustrate the difference between ionosphere AF and AK detectability, Fig. 4 shows a single-epoch, dual-frequency L1/L5 GPS example. This result clearly demonstrates the huge impact of the improvement-factor σ_p^2/σ_ϕ^2, when changing from the AF-detector to the AK-detector.

3 The ambiguity-resolved detector

3.1 Definition of AR-detector test

Strictly speaking, one cannot apply the AK test in case of GNSS. Although the ambiguities are known to be integer,

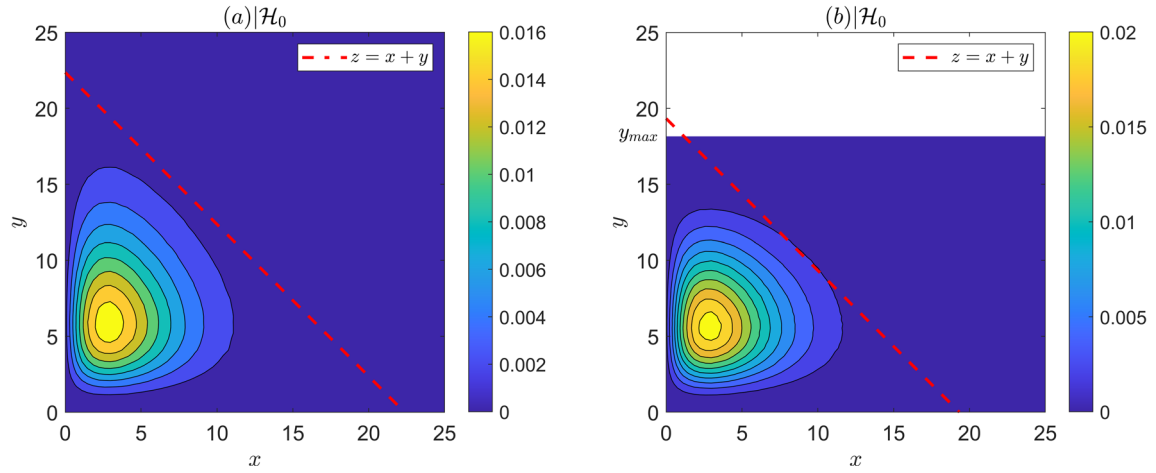

Fig. 5 Contour lines of the joint PDF under $\mathcal{H}_0$ of (a) $\underline{x} = ||\underline{\hat{e}}||^2_{Q_{yy}}$ and $\underline{y} = ||\underline{\hat{\epsilon}}(a)||^2_{Q_{\hat{a}\hat{a}}}$, and (b) $\underline{x} = ||\underline{\hat{e}}||^2_{Q_{yy}}$ and $\underline{y} = ||\underline{\check{\epsilon}}||^2_{Q_{\hat{a}\hat{a}}} = ||\hat{\epsilon}(\underline{\check{a}})||^2_{Q_{\hat{a}\hat{a}}}$, with $y_{\max} = 18.4$. The two red-dashed lines are the critical value lines corresponding to a false-alarm probability $\alpha = 0.05$, giving the critical values $z = 22.36$ for (a) and $z = 19.32$ for (b). The results are based on a single-epoch, dual-frequency L1/L5 GPS model, having an ILS success rate of $\mathsf{P}[\underline{\check{a}}_{\mathrm{ILS}} = a] = 62\%$, with $\#Sat = 5$, $r = 5$, $r(a) = 13$, $n = 8$, $\sigma_p = 0.5$ and $\sigma_\phi = 5$mm

they are still unknown. When the AK test is currently used in practice, the typical approach is to replace a by its integer estimate $\check{a}$, thereby treating *as if* it is the known ambiguity value. By replacing a in (8) by $\check{a}$, the test becomes

$$\text{AK}: \text{Reject } \mathcal{H}_0 \text{ if } ||\hat{e}(\check{a})||^2_{Q_{yy}} > \chi^2_\alpha(r(a), 0) \tag{24}$$

Due to the randomness of $\underline{\check{a}}$, however, this is now *not* the correct way of performing the test. It would only be correct if the ambiguity success rate, i.e. the probability of correct integer estimation $\mathsf{P}[\underline{\check{a}} = a]$, is sufficiently close to 1, thus allowing one to neglect the uncertainty in the integer estimator $\underline{\check{a}}$ and treating $||\hat{e}(\underline{\check{a}})||^2_{Q_{yy}}$ to be distributed under $\mathcal{H}_0$ as $\chi^2(r(a), 0)$. The first such application of the AK test, also in combination with the AF test, can be found in Chapter 8 of Teunissen and Kleusberg (1998). In the current contribution, however, we will do away with the restriction of the success rate being 1 and develop the corresponding ambiguity-resolved (AR) detector. The important practical advantage of releasing the restriction on the ambiguity success rate is that we will be able to perform an improved detection also for models for which the success rate may not be sufficiently close to 1. In doing so, we enable integer ambiguity resolution to serve two separate goals, namely (a) the goal of most precise parameter estimation for which the success rate has to be close to 1, and (b) the goal of improved model validation for which the success rate is not always required to be close to 1. The ambiguity-resolved detector is defined as follows.

Definition 2 (AR-Detector) Let $\underline{\check{a}} = \mathcal{I}(\underline{\hat{a}})$, $\mathcal{I}: \mathbb{R}^n \mapsto \mathbb{Z}^n$, be an *admissible* integer estimator of the mean of $\underline{\hat{a}} \overset{\mathcal{H}_0}{\sim} N_n(a \in \mathbb{Z}^n, Q_{\hat{a}\hat{a}})$, and let $\underline{\check{\epsilon}} = \hat{\epsilon}(\underline{\check{a}}) = \underline{\hat{a}} - \underline{\check{a}}$ be its corresponding ambiguity-residual vector. Then, the AR-detector test reads:

$$\text{Reject } \mathcal{H}_0 \text{ if } ||\check{e}||^2_{Q_{yy}} = ||\hat{e}||^2_{Q_{yy}} + ||\check{\epsilon}||^2_{Q_{\hat{a}\hat{a}}} > k_\alpha \tag{25}$$

and accept otherwise, with the critical value k_α providing the probability of false alarm (or level of significance) $\mathsf{P}[||\underline{\check{e}}||^2_{Q_{yy}} > k_\alpha | \mathcal{H}_0] = \alpha$. ■

To make an illustrative comparison between the AR-detector and the AK-detector, Fig. 5 shows an example of their acceptance regions and the contour lines of the joint PDF under $\mathcal{H}_0$ of $||\underline{\hat{e}}||^2_{Q_{yy}}$ and $||\underline{\hat{\epsilon}}(a)||^2_{Q_{\hat{a}\hat{a}}}$ (Fig. 5a), and the joint PDF under $\mathcal{H}_0$ of $||\underline{\hat{e}}||^2_{Q_{yy}}$ and $||\underline{\check{\epsilon}}||^2_{Q_{\hat{a}\hat{a}}} = ||\hat{\epsilon}(\underline{\check{a}})||^2_{Q_{\hat{a}\hat{a}}}$ (Fig. 5b). Comparison of the contour lines of these two joint PDFs shows that the one of Fig. 5b is somewhat compressed along the vertical axis. This is also clear when one compares the PDFs of $||\underline{\hat{\epsilon}}(a)||^2_{Q_{\hat{a}\hat{a}}}$ and $||\underline{\check{\epsilon}}||^2_{Q_{\hat{a}\hat{a}}}$, see Fig. 6(Top). As this compression also affects the cumulative distribution function (CDF) of the AR-detector, it can be used to explain its difference with that of the AK-detector. To do so, we first write the CDFs of the two detectors in a form that facilitates such comparison. As both $||\underline{\hat{\epsilon}}(a)||^2_{Q_{\hat{a}\hat{a}}}$ and $||\underline{\check{\epsilon}}||^2_{Q_{\hat{a}\hat{a}}}$ are independent of $||\underline{\hat{e}}||^2_{Q_{yy}}$, the PDFs of the two sums $||\underline{\hat{\epsilon}}(a)||^2_{Q_{yy}} = ||\underline{\hat{e}}||^2_{Q_{yy}} + ||\underline{\hat{\epsilon}}(a)||^2_{Q_{\hat{a}\hat{a}}}$ and $||\underline{\check{e}}||^2_{Q_{yy}} = ||\underline{\hat{e}}||^2_{Q_{yy}} + ||\underline{\check{\epsilon}}||^2_{Q_{\hat{a}\hat{a}}}$ can be written as *convolutions*. As a result, their CDFs can be written as an expectation of the CDF of the AF-detector, $F_{\mathrm{AF}}(x) = \mathsf{P}[||\underline{\hat{e}}||^2_{Q_{yy}} \leq x]$. We therefore may write the CDFs of the AK- and AR-detector as

$$\begin{aligned} F_{\mathrm{AK}}(x) &= \mathsf{E}_{||\underline{\hat{\epsilon}}(a)||^2_{Q_{\hat{a}\hat{a}}}}[F_{\mathrm{AF}}(x - ||\underline{\hat{\epsilon}}(a)||^2_{Q_{\hat{a}\hat{a}}})] \\ F_{\mathrm{AR}}(x) &= \mathsf{E}_{||\underline{\check{\epsilon}}||^2_{Q_{\hat{a}\hat{a}}}}[F_{\mathrm{AF}}(x - ||\underline{\check{\epsilon}}||^2_{Q_{\hat{a}\hat{a}}})], \end{aligned} \tag{26}$$

thus showing that the difference between the AK- and AR-CDF lies in the different weighting of the AF-CDF, i.e. $\mathsf{E}_{||\underline{\hat{\epsilon}}(a)||^2_{Q_{\hat{a}\hat{a}}}}[.]$ versus $\mathsf{E}_{||\underline{\check{\epsilon}}||^2_{Q_{\hat{a}\hat{a}}}}[.]$. As the PDF inequality $f_{||\underline{\check{\epsilon}}||^2_{Q_{\hat{a}\hat{a}}}}(y) \geq f_{||\underline{\hat{\epsilon}}(a)||^2_{Q_{\hat{a}\hat{a}}}}(y)$ holds true for the smaller range of y-values (cf. Figure 6 (Top)), the CDF function values $F_{\mathrm{AF}}(x-y)$ get more weighted by $f_{||\underline{\check{\epsilon}}||^2_{Q_{\hat{a}\hat{a}}}}(y)$ when $x-y$ is closer to x then when it is much smaller than x. This combined with the fact that the AF-CDF is a monotone increasing function explains why in Fig. 6 (Bottom) the function values of the AR-CDF lie above those of the AK-CDF, $F_{\mathrm{AR}}(x) \geq F_{\mathrm{AK}}(x)$.

3.2 AR-detector under $\mathcal{H}_0$

The difference between the AK- and AR-detector lies in the replacement of $\underline{\hat{\epsilon}}(a)$ by $\underline{\check{\epsilon}} = \hat{\epsilon}(\check{a})$. Hence, to gain further insight into the probabilistic properties of the AR-detector, we need to know those of $\underline{\check{\epsilon}}$. The PDF of $\underline{\check{\epsilon}}$ was first given in Teunissen (2002) as

$$f_{\underline{\check{\epsilon}}}(x) = \frac{\sum_{z\in\mathbb{Z}^n} \exp\{-\frac{1}{2}||x+z||^2_{Q_{\hat{a}\hat{a}}}\}}{\sqrt{|2\pi\, Q_{\hat{a}\hat{a}}|}} s_0(x) \tag{27}$$

in which $s_0(x)$ is the indicator function of the integer estimator's *pull-in region* S_0, i.e.

$$s_0(x) = \begin{cases} 1 \text{ if } x \in S_0 \\ 0 \text{ otherwise} \end{cases} \tag{28}$$

The pull-in regions of IR, IB and ILS are given as,

$$\begin{aligned} S_{0,\mathrm{IR}} &= \{x \in \mathbb{R}^n |\ |c_i^T x| \leq \tfrac{1}{2}, i = 1,\ldots,n\} \\ S_{0,\mathrm{IB}} &= \{x \in \mathbb{R}^n |\ |c_i^T L^{-1} x| \leq \tfrac{1}{2}, i = 1,\ldots,n\} \\ S_{0,\mathrm{ILS}} &= \{x \in \mathbb{R}^n |\ |z^T Q_{\hat{a}\hat{a}}^{-1} x| \leq \tfrac{1}{2}||z||^2_{Q_{\hat{a}\hat{a}}}, \forall z \in \mathbb{Z}^n\} \end{aligned}$$

in which L is the unit-triangular matrix of the triangular decomposition $Q_{\hat{a}\hat{a}} = LDL^T$ and c_i denotes the canonical unit vector having a 1 as its ith entry and zeros otherwise, see, for example, Chapter 23 of Teunissen and Montenbruck (2017). In two dimensions, these pull-in regions are, respectively, a unit square, a parallelogram and a hexagon. Figure 7 shows a two-dimensional example of the contour lines of $f_{\underline{\check{\epsilon}}}(x)$ for IR, IB and ILS, whereby the top row is for a highly correlated $\underline{\hat{a}}$ and the bottom row for its LAMBDA-decorrelated form (Teunissen, 1995).

An important property of the ambiguity residual is that it is always limited by its own pull-in region, $\underline{\check{\epsilon}} \in S_0$. This implies that the squared weighted-norm of the ambiguity residual, $||\underline{\check{\epsilon}}||^2_{Q_{\hat{a}\hat{a}}}$, is bounded. The largest value it can take is

$$\rho^2 = \max_{x\in S_0} ||x||^2_{Q_{\hat{a}\hat{a}}} \tag{29}$$

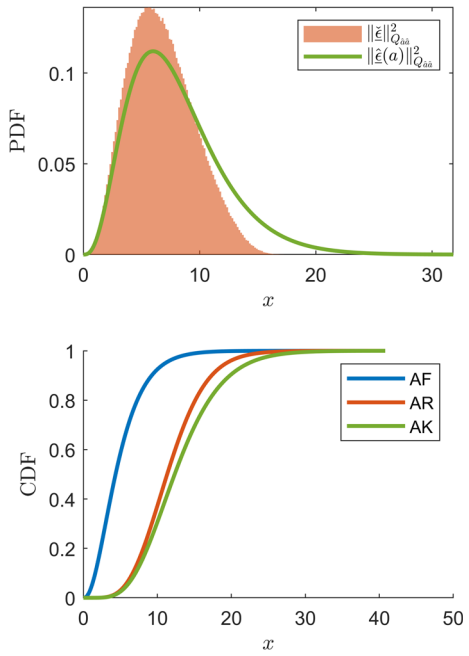

Fig. 6 (Top) $\mathcal{H}_0$-PDFs of $||\underline{\check{\epsilon}}||^2_{Q_{\hat{a}\hat{a}}}$ and $||\underline{\hat{\epsilon}}(a)||^2_{Q_{\hat{a}\hat{a}}}$; (Bottom) $\mathcal{H}_0$-CDFs of the AF-, AR- and AK-detector. The underlying model is a dual-frequency GPS model having a 62% ambiguity success rate

Thus, ρ is the largest distance, in the metric of $Q_{\hat{a}\hat{a}}$, that a point in the pull-in region S_0 can have to the origin. Alternatively, ρ^2 can be said to describe the smallest origin-centred ellipsoid $||x||^2_{Q_{\hat{a}\hat{a}}} =$ constant that covers the whole of S_0. For instance, $\rho = \frac{1}{2}\sqrt{n}$, in case S_0 is the unit-hypercube and $Q_{\hat{a}\hat{a}} = I_n$.

The boundedness of $||\underline{\check{\epsilon}}||^2_{Q_{\hat{a}\hat{a}}}$ (see Fig. 5b) implies that all the probability mass of its distribution is confined to the interval $[0, \rho^2]$, while that of the chi-square distributed $||\underline{\hat{\epsilon}}(a)||^2_{Q_{\hat{a}\hat{a}}}$ is spread over $[0, \infty)$. This compression of the probability mass to a smaller region, may lead, in dependence of its spread, to a critical value that is smaller than the one of the AK-detector, $k_\alpha \leq \chi^2_\alpha(r(a), 0)$. This is certainly the case when the AK-detector is computed with a being an integer and the AR-detector with $\check{a}$ being the ILS ambiguity estimate, since then $||\hat{\epsilon}(\check{a})||^2_{Q_{\hat{a}\hat{a}}} \leq ||\hat{\epsilon}(a)||^2_{Q_{\hat{a}\hat{a}}}, \forall a \in \mathbb{Z}^n$ (see Fig. 5b).

Another important characteristic difference between the AK-detector and AR-detector is that the PDF of the former under $\mathcal{H}_0$ does *not* depend on the precision of the ambiguity vector $\underline{\hat{a}}$ (i.e. as it is $\chi^2(r(a), 0)$-distributed, it only depends on the degrees of freedom $r(a)$), while the PDF of the latter does. To see this, let $Q_{\hat{a}\hat{a}} = \sigma^2 Q$ and consider the PDF of $\frac{1}{\sigma}\underline{\check{\epsilon}}$ in $||\underline{\check{\epsilon}}||^2_{Q_{\hat{a}\hat{a}}} = ||\frac{1}{\sigma}\underline{\check{\epsilon}}||^2_Q$. Since $f_{\frac{1}{\sigma}\underline{\check{\epsilon}}}(x) = \sigma f_{\underline{\check{\epsilon}}}(\sigma x)$, we have according to (27),

$$f_{\frac{1}{\sigma}\underline{\check{\epsilon}}}(x) = \frac{\sum_{z\in\mathbb{Z}^n} \exp\{-\frac{1}{2}||x+\frac{z}{\sigma}||^2_Q\}}{\sqrt{|2\pi\, Q|}} s_0(\sigma x) \tag{30}$$

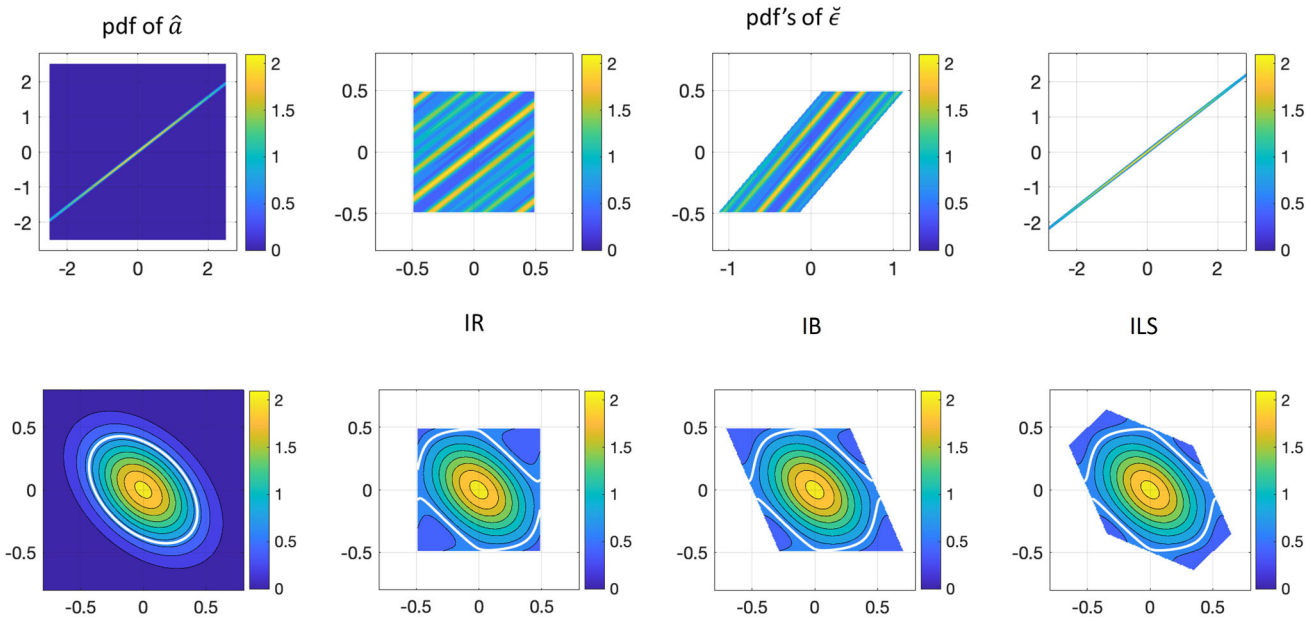

Fig. 7 Contour lines of PDFs of $\underline{\hat{a}}$ and $\underline{\check{\epsilon}}$ for three different integer estimators (IR, IB, ILS), when ambiguities are in double-differenced form (top row) and LAMBDA-decorrelated form (bottom row), after (Teunissen and Verhagen 2023)

with

$$s_0(\sigma x) = \begin{cases} 1 \text{ if } x \in \frac{1}{\sigma} S_0 \\ 0 \text{ otherwise} \end{cases} \tag{31}$$

thus showing that the PDF of $\frac{1}{\sigma}\underline{\check{\epsilon}}$, and therefore that of $||\frac{1}{\sigma}\underline{\check{\epsilon}}||^2_Q$ still depends on σ.

This dependence on σ also implies that $||\underline{\check{\epsilon}}||^2_{Q_{\hat{a}\hat{a}}}$ has quite different PDFs when σ of $Q_{\hat{a}\hat{a}} = \sigma^2 Q$ varies, and in particular when it goes to zero or to infinity. When σ goes to zero, the pull-in region (31) increases in size to cover the whole of $\mathbb{R}^n$, while the influence of the nonzero integers in the sum of (30) disappears. Therefore, $\lim_{\sigma\to 0} f_{\frac{1}{\sigma}\underline{\check{\epsilon}}}(x) = \mathcal{N}_n(0, Q)$ and $\lim_{\sigma\to 0} f_{||\frac{1}{\sigma}\underline{\check{\epsilon}}||^2_Q}(x) = \chi^2(n, 0)$, thus showing that $\lim_{\sigma\to 0} f_{||\underline{\check{\epsilon}}||^2_{Q_{\hat{a}\hat{a}}}}(x) = \chi^2(r(a), 0)$ Hence, the more precise the ambiguities become, the more the AR-detector will behave like the AK-detector. On the other hand, when σ goes to infinity, the pull-in region (31) reduces to a single point, the origin, over which all probability masses get concentrated, thus turning the density function into an impulse function. Therefore we have, $\lim_{\sigma\to\infty} f_{\frac{1}{\sigma}\underline{\check{\epsilon}}}(x) = \delta(x)$ and $\lim_{\sigma\to\infty} f_{||\underline{\check{\epsilon}}||^2_{Q_{\hat{a}\hat{a}}}}(x) = \delta(x)$, which upon substitution into $F_{\text{AR}}(x) = \mathsf{E}_{||\underline{\check{\epsilon}}||^2_{Q_{\hat{a}\hat{a}}}}[F_{\text{AF}}(x - ||\underline{\check{\epsilon}}||^2_{Q_{\hat{a}\hat{a}}})]$ (cf. 26) shows that when ambiguities get less precise, in the limit $F_{\text{AR}}(x) = F_{\text{AF}}(x)$, i.e. the AR-detector will then behave like the AF-detector.

3.3 On the invariance of the AR-detector

We have seen that the AF-detector is incapable of detecting model biases Cc when $\mathcal{R}(C) \subset \mathcal{R}([A, B])$. Similarly, the AK-detector is incapable of detecting model biases when $\mathcal{R}(C) \subset \mathcal{R}(B)$. To determine a likewise invariance for the AR-detector, we parametrize the model bias in $\underline{y}|\mathcal{H}_a = \underline{y}|\mathcal{H}_0 + Cc$ as $Cc = \bar{A}\alpha + B\beta + [A, B]^{\perp}\gamma$ and infer for which of its components the AR-detector $||\underline{\check{e}}||^2_{Q_{yy}} = ||\underline{\hat{e}}||^2_{Q_{yy}} + ||\underline{\check{\epsilon}}||^2_{Q_{\hat{a}\hat{a}}}$ remains invariant (note: the here used parametrization in vectors α and γ should not be confused with the used notation for level of significance (α) and power (γ)). As $||\underline{\hat{e}}||^2_{Q_{yy}}$ is invariant for $\bar{A}\alpha + B\beta$, and $\underline{\check{\epsilon}} = \underline{\hat{a}} - \mathcal{I}(\underline{\hat{a}})$, with $\underline{\hat{a}} = \bar{A}^+\underline{y}$, is invariant for $B\beta$, we only need to consider whether $\underline{\check{\epsilon}} = \underline{\hat{a}} - \mathcal{I}(\underline{\hat{a}})$ has an additional invariance for certain biases $\bar{A}\alpha$. This indeed is the case. From the *integer equivariance* $\mathcal{I}(x + z) = \mathcal{I}(x) + z$, $\forall z \in \mathbb{Z}^n$, it follows that $\bar{A}^+(\underline{y}|\mathcal{H}_0 + \bar{A}\alpha) - \mathcal{I}(\bar{A}^+(\underline{y}|\mathcal{H}_0 + \bar{A}\alpha))$ is invariant for any integer vector α. The conclusion reads therefore that in the comparison with the AK-detector, the AR-detector exhibits an important additional invariance. The invariance of the three detectors can therefore be summarized as follows:

Lemma 3 *(*Invariance of AF-, AK-, AR-detector*) Let the model bias Cc perturb the observational vector as $\underline{y}|\mathcal{H}_a = \underline{y}|\mathcal{H}_0 + Cc$. Then, the detectors exhibit the following invariance under this perturbation:*

$$\begin{array}{ll} \text{AF invariant for } Cc = \bar{A}\alpha + B\beta, \forall \alpha \in \mathbb{R}^n, \beta \in \mathbb{R}^p \\ \text{AK invariant for } Cc = \quad B\beta, \forall \beta \in \mathbb{R}^p \\ \text{AR invariant for } Cc = \bar{A}z + B\beta, \forall z \in \mathbb{Z}^n, \beta \in \mathbb{R}^p \end{array} \tag{32}$$

■

Note although the AF-invariance looks similar to the AR-invariance, that the former extends to a complete $(n + p)$-dimensional linear space $\mathcal{R}(\bar{A}, B)$, while that of the latter is confined to p-dimensional *parallel* spaces, obtained by translation over all grid points $\bar{A}z$, $z \in \mathbb{Z}$, i.e. $\bar{A}z + \mathcal{R}(B)$. Thus, if $\bar{A}z$ forms a *dense* grid in $\mathbb{R}^m$, one can expect the AR-invariance to be similar to the AF-invariance. Their invariance will significantly differ, however, when the grid is sparse, in which case the AR-invariance will more closely resemble that of the AK-invariance. A scalar measure of the denseness of $\bar{A}z, z \in \mathbb{Z}$, is provided by the ambiguity dilution of precision (ADOP) (Teunissen 1997),

$$\text{ADOP} = |\bar{A}^T Q_{yy}^{-1} \bar{A}|^{-\frac{1}{2n}} \quad \text{(cycle)} \tag{33}$$

The smaller the ADOP, the less dense the grid spacing of $\bar{A}z$ is in relation to the metric Q_{yy}^{-1} of observation space.

To illustrate the fundamental difference between the two different types of invariance of the AF- and AR-detector, the following example describes a case for which the bias is not detectable with the AF-detector, but is detectable with the AR-detector, except for certain special discrete bias values.

Example (Code-bias in geometry-free model): As null hypothesis we consider the single-epoch, f-frequency, short baseline geometry-free DD model

$$\mathsf{E}\begin{bmatrix} \underline{p} \\ \underline{\phi} \end{bmatrix} = \underbrace{\begin{bmatrix} 0 & e_f \\ \Lambda & e_f \end{bmatrix}}_{A \quad B} \begin{bmatrix} a \\ \rho \end{bmatrix}, \quad \mathsf{D}\begin{bmatrix} \underline{p} \\ \underline{\phi} \end{bmatrix} = \begin{bmatrix} \sigma_p^2 I_f & 0 \\ 0 & \sigma_\phi^2 I_f \end{bmatrix} \tag{34}$$

with $\underline{p}, \underline{\phi} \in \mathbb{R}^f$ the DD pseudorange and carrier-phase observational vectors, $a \in \mathbb{Z}^f$ the unknown integer ambiguity vector, $\rho \in \mathbb{R}$ the unknown DD range, $\Lambda = \text{diag}[\lambda_1, \ldots, \lambda_f]$ the diagonal matrix of f wavelengths and $e_f = [1, \ldots, 1]^T$ the f-vector of ones. If we now assume that under the alternative hypothesis all pseudoranges are biased with the same bias, then

$$Cc = \begin{bmatrix} e_f \\ 0 \end{bmatrix} c \tag{35}$$

Such bias is detectable with the AK-detector, i.e. when the ambiguity vector a is assumed known. However, since (35) is linear dependent on the $f+1$ column vectors of the design matrix of (34), i.e.

$$\begin{bmatrix} 0 & e_f & e_f \\ \Lambda & e_f & 0 \end{bmatrix} \begin{bmatrix} -\Lambda^{-1} e_f \\ -1 \\ 1 \end{bmatrix} = \begin{bmatrix} 0 \\ 0 \end{bmatrix} \tag{36}$$

the bias (35) is *not* detectable with the AF-detector. To find out under what circumstances the bias is detectable with the AR-detector, we need to solve the equation $Cc = \bar{A}\alpha + B\beta$ and infer for what values of c the solution α is integer. For model (34), we have

$$\bar{A} = P_B^\perp A = \begin{bmatrix} -\frac{1}{1+\epsilon} P_{e_f} \\ I_f - \frac{1}{1+\epsilon} P_{e_f} \end{bmatrix} \Lambda, \quad B = \begin{bmatrix} e_f \\ e_f \end{bmatrix} \tag{37}$$

with projector $P_{e_f} = e_f (e_f^T e_f)^{-1} e_f^T$ and phase-code variance ratio $\epsilon = \sigma_\phi^2 / \sigma_p^2$. From solving the equation $Cc = \bar{A}\alpha + B\beta$, it follows that α is integer if and only if

$$c = \lambda_1 z_1 = \lambda_2 z_2 = \ldots = \lambda_f z_f \tag{38}$$

for some $z_i \in \mathbb{Z}$, $i = 1, \ldots, f$. The conclusion reads therefore that in contrast to the AF-detector, the bias (35) is detectable with the AR-detector, except in the very special cases when the bias equals an integer multiple of the wavelengths. Thus in the single-frequency case, the smallest bias for which this would happen would be $c = \pm\lambda_1$. This value rapidly increases when more frequencies are used. In the dual-frequency GPS case, for instance, where $\lambda_2/\lambda_1 = 77/60$, the smallest bias for which no AR-detection would be possible is already $c = \pm 77\lambda_1$. □

A consequence of the above identified invariance of the AR-detector is that it impacts the behaviour of its power function. To see this, we make use of the independence of $\underline{x} = ||\underline{\hat{e}}||^2_{Q_{yy}}$ and $||\hat{\epsilon}(\underline{\check{a}})||^2_{Q_{\hat{a}\hat{a}}}$, and of the continuous version of the total probability rule, to write the AR-power function as

$$\begin{aligned} \gamma_{\text{AR}} &= \mathsf{P}[||\underline{\hat{e}}||^2_{Q_{yy}} + ||\hat{\epsilon}(\underline{\check{a}})||^2_{Q_{\hat{a}\hat{a}}} > k_\alpha | \mathcal{H}_a] \\ &= \int \mathsf{P}[||\hat{\epsilon}(\check{a})||^2_{Q_{\hat{a}\hat{a}}} > k_\alpha(x) | \mathcal{H}_a] f_{\underline{x}}(x|\mathcal{H}_a) dx \end{aligned} \tag{39}$$

in which $k_\alpha(x) = k_\alpha - x$. This shows that the power γ_{AR} can be interpreted as being the *expectation* of the following function of the noncentral chi-square distributed random variable $\underline{x} = ||\underline{\hat{e}}||^2_{Q_{yy}}$: $\mathsf{P}[||\hat{\epsilon}(\check{a})||^2_{Q_{\hat{a}\hat{a}}} > k_\alpha(\underline{x}) | \mathcal{H}_a]$. The impact of the model bias Cc for which the AF-detector is sensitive, is captured in the noncentral chi-square PDF $f_{\underline{x}}(x|\mathcal{H}_a)$, while the additional bias sensitivity of the AR-detector, namely $\bar{A}^+ Cc \notin \mathbb{Z}^n$, is captured by the probability function inside the integral of (39). With the z-centred ellipsoid $E_z = \{u \in \mathbb{R}^n | ||u - z||^2_{Q_{\hat{a}\hat{a}}} \leq k_\alpha(x)\}$ and the z-centred pull-in region $S_z = \{u \in \mathbb{R}^n | z = \mathcal{I}(u)\}$ of the integer estimator used, the complement of this probability can be worked out to give

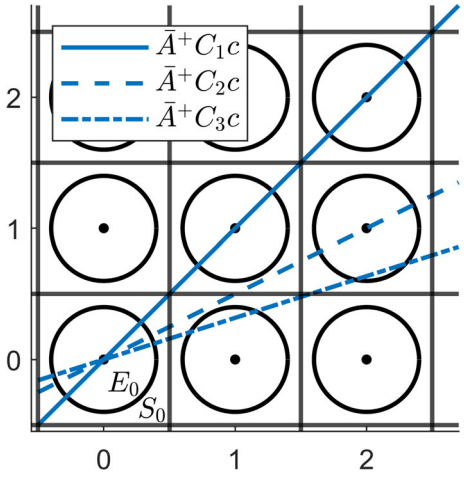

Fig. 8 Three different model bias lines, $\bar{A}^+C_1c \in \mathbb{R}^2$, $\bar{A}^+C_2c \in \mathbb{R}^2$ and $\bar{A}^+C_3c \in \mathbb{R}^2$, with 2D integer grid $\mathbb{Z}^2$, showing pull-in regions S_z as unit squares and $E_z \subset S_z$ as circular regions. The model bias lines $\bar{A}^+C_1c \in \mathbb{R}^2$ and $\bar{A}^+C_2c \in \mathbb{R}^2$ both pass through integer grid points (e.g. $[1, 1]^T z$ and $[2, 1]^T z$, $z \in \mathbb{Z}$), while model bias line $\bar{A}^+C_3c \in \mathbb{R}^2$ does not

$$
\begin{aligned}
&\mathsf{P}[||\hat{\epsilon}(\breve{a})||^2_{Q_{\hat{a}\hat{a}}} \le k_\alpha(x)|\mathcal{H}_a] = \\
&\overset{(1)}{=} \sum_{z\in\mathbb{Z}^n} \mathsf{P}[||\underline{\hat{\epsilon}}(z)||^2_{Q_{\hat{a}\hat{a}}} \le k_\alpha(x), \underline{\hat{a}} \in S_z|\mathcal{H}_a] \\
&\overset{(2)}{=} \sum_{z\in\mathbb{Z}^n} \mathsf{P}[||\underline{\hat{a}} - z||^2_{Q_{\hat{a}\hat{a}}} \le k_\alpha(x), \underline{\hat{a}} \in S_z|\mathcal{H}_a] \\
&\overset{(3)}{=} \sum_{z\in\mathbb{Z}^n} \mathsf{P}[\underline{\hat{a}} \in E_z \cap S_z|\mathcal{H}_a] \\
&\overset{(4)}{=} \sum_{z\in\mathbb{Z}^n} \mathsf{P}[\underline{\hat{a}} + \bar{A}^+Cc \in E_z \cap S_z|\mathcal{H}_0]
\end{aligned}
\tag{40}
$$

Step (1) follows from using the property that pull-in regions cover the complete space $\mathbb{R}^n$ without gaps and overlaps, while step (2) uses the equivalence $\underline{\hat{a}} \in S_z \Leftrightarrow \breve{a} = z$, and step (3) formulates the overlap of the z-centred ellipsoid and pull-in region as an intersection. Finally, step (4) makes use of the property that if the alternative hypothesis is true, the float ambiguity estimator computed under the null hypothesis is biased by $\bar{A}^+Cc$.

To provide a qualitative description of how the above probability (40) depends on the model bias, Fig. 8 illustrates a 2D example with three different model bias lines, $\bar{A}^+C_1c$, $\bar{A}^+C_2c$ and $\bar{A}^+C_3c$. For simplicity, we assumed the ambiguity variance matrix to be a scaled unit-matrix, thus resulting in pull-in regions S_z being unit squares and the ellipsoids E_z being circular regions. Note that the lines $\bar{A}^+C_1c$ and $\bar{A}^+C_2c$ pass through integer grid points $[1, 1]^T z$ and $[2, 1]^T z$, for $z \in \mathbb{Z}$, while the third line $\bar{A}^+C_3c$ does not pass through integer grid points. The value of the probability (40) depends now on where the $\mathcal{H}_0$-PDF of $\underline{\hat{a}}$ is centred along those bias lines.

Probability (40) is largest when the $\mathcal{H}_0$-PDF of $\underline{\hat{a}}$ is centred at the origin. Would it then move away from the origin and pass over the model bias line $\bar{A}^+C_1c$, the probability would in the beginning decrease, then reach its minimum when the centre of the PDF has equal distances to the four nearest grid points, after which the probability increases again until the centre of the PDF is again over an integer grid point, in this case $[1, 1]^T$. As this same behaviour repeats when the centre of the PDF continuous along the line $\bar{A}^+C_1c$, the probability (40) will show a periodic behaviour as function of increasing c. Such periodic behaviour, with possibly different periods, will occur for any bias line that passes through an integer grid point. The bias line $\bar{A}^+C_2c$, for instance, also passes through integer grid points but which now are at a greater distance from each other. Such periodic behaviour will *not* occur when the $\mathcal{H}_0$-PDF of $\underline{\hat{a}}$ moves along a bias line that has no integer grid points on it, e.g. $\bar{A}^+C_3c$ of Fig. 8. But despite this absence of periodicity, the probability will then still not change in a monotonic manner when the centre of the PDF moves away from the origin. Although the probability mass of the PDF over E_0 will decrease when moving away from the origin, it may after a while again pick up more probability mass from some of the other $E_{z\neq 0}$.

As the above-described variable behaviour of probability (40) propagates into the expectation integral of (39), the AR-power function will not be a monotonic function. It will fluctuate in dependence on how close the ambiguity bias $\bar{A}^+Cc$ is to an integer. The frequency and size of these fluctuations is driven by the combined effect of the denseness of the grid (i.e. the ADOP, cf. 33) and the size of the input bias c with its impact on the noncentrality parameter of the weighting function $f_{\underline{x}}(x|\mathcal{H}_a)$ (cf. 39). As the impact on the latter will increase with increasing input bias, the fluctuations will have the general tendency of dying out when c increases.

To illustrate the above findings and to compare the detection performance of the AR-detector with that of the AK- and AF-detector, Fig. 9 shows the power function curves of the three detectors for the same receiver-satellite geometry of Fig. 4. Four different cases are shown: (a) dual-frequency L1/L5 with $\sigma_p = 50$cm; (b) dual-frequency L1/L5 with $\sigma_p = 20$cm; (c) triple-frequency L1/L2/L5 with $\sigma_p = 50$cm; and (d) triple-frequency L1/L2/L5 with $\sigma_p = 20$cm. In all cases, the standard deviations are undifferenced values and the phase standard deviation is $\sigma_\phi = 2$mm. Thus, (a) and (c) may represent a mass-market receiver, while (b) and (d) may represent a geodetic receiver. The weakest model is that of (a), while the strongest model is that of (d). In all cases, we see how the AR-detector outperforms the AF-detector. This is already the case with the weakest model (a) having an ambiguity success rate of only 88%. For instance, for $c \approx 20$, with $\alpha = 0.05$, the power of the AR-detector is about 80%, while that of the AF-detector is only 50%. This is thus a situation for which the model strength would not be enough to perform integer ambiguity resolution for parameter estimation, but good enough to get a better detection performance

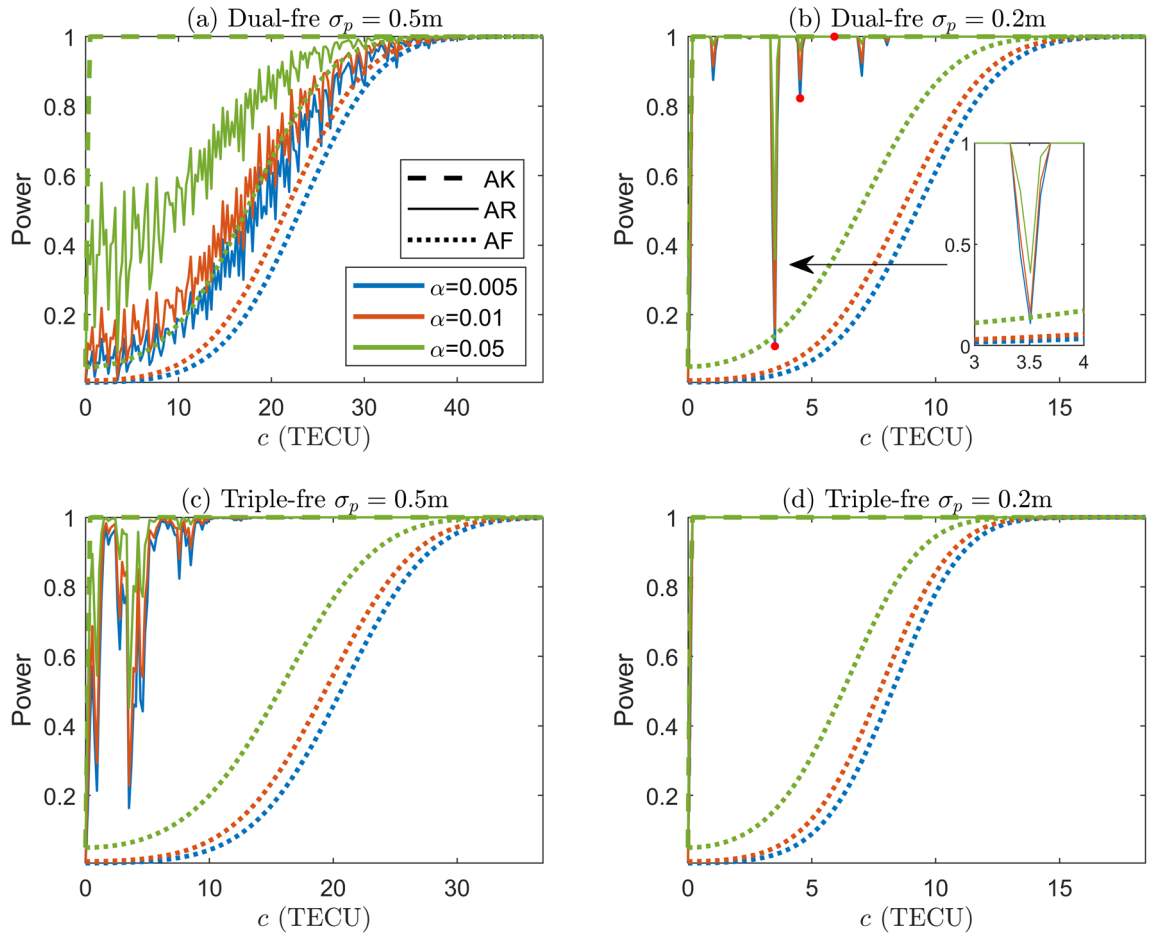

Fig. 9 AR-, AK- and AF-power function curves for ionosphere detection as function of iono-delay in TEC units, for a single-epoch GPS model, with different false-alarm probabilities (levels of significance α): (a) Dual-frequency L1/L5, $\sigma_p = 50$cm; (b) Dual-frequency L1/L5, $\sigma_p = 20$cm; (c) Triple-frequency L1/L2/L5, $\sigma_p = 50cm$; and (d) Triple-frequency L1/L2/L5, $\sigma_p = 20cm$

with the use of the ambiguity-resolved detector than with the ambiguity-float detector.

For the weakest model (a), having the densest integer grid, we also see clearly, as predicted, the rapid fluctuations in the AR-power function, which die out for increasing c. When the integer grid gets less dense, the fluctuations will be less rapid. The detection power increases when the model becomes stronger. This is clear for the mass-market receiver, when an additional frequency is added, i.e. compare (a) with (c). And it is also clear for the dual-frequency scenario, when the pseudorange precision improves from $\sigma_p = 50$cm to $\sigma_p = 20$cm, i.e. compare (a) with (b). Note the tremendous increase in AR-detection power that this improvement in pseudorange precision achieves (also note thereby the difference in horizontal scale). Except for a few cases, the realized performance is almost that of what the AK-detector would bring were it an operational detector. The occurrences, however, of these few cases, where the power suddenly drops in value, are important to identify. As explained earlier, these sudden drops happen when $\bar{A}^+Cc$ gets close to an integer vector (cf. Fig. 8). With $\mathcal{I} : \mathbb{R}^n \mapsto \mathbb{Z}^n$ being the ILS-map, the distance of $\bar{A}^+Cc$ to the nearest integer vector is given by

$$D(c) = ||\bar{A}^+Cc - \mathcal{I}(\bar{A}^+Cc)||_{Q_{\hat{a}\hat{a}}} \tag{41}$$

Thus, the smaller this distance, the larger one can expect the drop in power to be. To illustrate this, we have chosen three cases, $c_1 = 3.5$ TECU, $c_2 = 4.5$ TECU and $c_3 = 5.9$ TECU, identified in Fig. 9b by three red dots. Their distance to their nearest integer vector was computed as $D(c_1) = 2.57 < D(c_2) = 5.44 < D(c_3) = 9.19$, thus indeed explaining why the detection power in these three cases is so different. It will be clear if one would be relying on the performance description of the AK-detector that one would be getting a very deceptive description of the detection power in these cases. This is therefore another pitfall would one work with the AK-detector statistics.

3.4 On computing the AR-power function

In order to be able to evaluate the performance of the AR-detector for any particular application, one needs an efficient way to compute its power function. Our previous integral expression (39), that we used to obtain a qualitative insight into the behaviour of the power function, is, however, not really suited for this task. Therefore, we make use of the AR-CDF expression (26), which under $\mathcal{H}_a$ can be written as

$$F_{\mathrm{AR}}(x|\mathcal{H}_a) = \mathsf{E}_{\underline{\check{y}}}[F_{\mathrm{AF}}(x - \underline{\check{y}}|\mathcal{H}_a)] \tag{42}$$

with $\underline{\check{y}} = ||\underline{\check{e}}|\mathcal{H}_a||^2_{Q_{\hat{a}\hat{a}}}$. The corresponding expression for the power follows then as

$$\begin{aligned}\gamma_{\mathrm{AR}} &= 1 - F_{\mathrm{AR}}(k_\alpha|\mathcal{H}_a)\\ &= \mathsf{E}_{\underline{\check{y}}}[1 - F_{\mathrm{AF}}(k_\alpha - \underline{\check{y}}|\mathcal{H}_a)]\\ &= \mathsf{E}_{\underline{\check{y}}}[\mathsf{P}[\underline{\chi}^2(r, \lambda_{\hat{e}}) \geq k_\alpha - \underline{\check{y}}]\end{aligned} \tag{43}$$

which, as the last expression shows, has the advantage that a chi-square calculator can be used in its calculations. The calculation and simulation steps that need to be followed for the construction of an AR-power function can now be summarized as follows:

1. First formulate the alternative hypothesis $\underline{y} \overset{\mathcal{H}_a}{\sim} N_m(Aa + Bb + Cc, Q_{yy})$, $a \in \mathbb{Z}^n$, by specifying, through Cc, the type of model bias one wants to consider.
2. Then, infer the impact this bias has on $||\underline{\hat{e}}||^2_{Q_{yy}}$ and $\underline{\hat{a}}$. This is done by computing the noncentrality parameter $\lambda_{\hat{e}} = ||P^{\perp}_{[A,B]}Cc||^2_{Q_{yy}}$ of $||\underline{\hat{e}}||^2_{Q_{yy}} \overset{\mathcal{H}_a}{\sim} \underline{\chi}^2(r, \lambda_{\hat{e}})$ and the ambiguity bias $\bar{A}^+Cc$ in $\underline{\hat{a}} \overset{\mathcal{H}_a}{\sim} f_{\underline{\hat{a}}}(x|\mathcal{H}_a) = N_m(a + \bar{A}^+Cc, Q_{\hat{a}\hat{a}})$.
3. From a Monte Carlo simulation of N idd samples $\hat{a}_i, i = 1, \ldots, N$, of the PDF $f_{\underline{\hat{a}}}(x|\mathcal{H}_a)$, the N corresponding ambiguity-residual samples $\check{\epsilon}_i = \hat{a}_i - \check{a}_i$ are constructed. Hereby the user needs to make a choice which admissible integer estimator to use. In case of the ILS-estimator, the samples $\check{a}_i = \arg\min_{z\in\mathbb{Z}^n} ||\hat{a}_i - z||^2_{Q_{\hat{a}\hat{a}}}$ are computed by means of the LAMBDA-method (Teunissen 1995). For the choice of N, use is made of the accuracy assessment method described in Morio and Balesdent (2015).
4. By using the chi-square calculator and approximating the expectation of (43) with the numerical average of the generated samples, the power is finally computed as

$$\gamma_{\mathrm{AR}} := \tfrac{1}{N}\sum_{i=1}^{N} \mathsf{P}[\underline{\chi}^2(r, \lambda_{\hat{e}}) \geq k_\alpha - ||\check{\epsilon}_i||^2_{Q_{\hat{a}\hat{a}}}]$$

As the above procedure requires the critical value k_α as input, a separate prior simulation is carried out to determine k_α from the user-defined value of $1 - \alpha = F_{\mathrm{AR}}(k_\alpha|\mathcal{H}_0) = \mathsf{P}[||\underline{\check{e}}||^2_{Q_{\hat{a}\hat{a}}} \leq k_\alpha|\mathcal{H}_0]$. This entails executing a similar simulation as above, but now for $||\underline{\check{e}}||^2_{Q_{\hat{a}\hat{a}}}$ under $\mathcal{H}_0$. After the samples $||\underline{\check{e}}_i||^2_{Q_{\hat{a}\hat{a}}}$ are put in ascending order, k_α is taken as the rounded value of the $(1 - \alpha)N$th ordered sample.

4 Summary and conclusions

In this contribution, we introduced the ambiguity-resolved (AR) detector and studied its characteristics. The AR-detector is a new detector that lies in between the ambiguity-float (AF) detector and the ambiguity-known (AK) detector. The AF-detector treats the ambiguity vector as unknown, while the AK-detector assumes the ambiguity vector to be known completely. As the ambiguity vector can seldomly be known completely, the AK-detector is not an operational detector, thus implying that reliance on its properties will be incorrect. The AR-detector resolves the shortcomings of the AK-detector by treating the ambiguities as unknown integers. As such, it is designed to work as the detector for mixed-integer GNSS models.

To gain insight in the relative detection properties, we first compared the detection capabilities of the AF- and AK-detector. This was then further made explicit for the mixed-integer GNSS model by developing expressions for the noncentrality parameters of the detectors. This was done in dependence of four different type of model biases (code-type, phase-type, tropo-type and iono-type), thus revealing under which circumstances which model biases would find improved detection if the ambiguities would be known. As such, these results provided a first indication of the improvements one can expect to gain from the AR-detector.

Following the above analysis, we studied and compared the distributional properties (PDF and CDF) of the AR- and AK-detector. Special attention was hereby given to the impact of the probability mass function of the integer resolved ambiguities. An important aspect hereby concerns the different properties of invariance that the detectors exhibit. With $[A, B]$ being the design matrix under the null hypothesis, the AK-detector is only invariant for model biases that reside in the range space of B. This is also true for the AR-detector, except for the special case when the model bias has a component coinciding with one of the grid points $\bar{A}z$, $z \in \mathbb{Z}^n$. For those special cases, it exhibits the same invariance as the AF-detector. Thus, if $\bar{A}z$ forms a sufficiently sparse grid, one can expect the AR-detector to outperform the commonly used AF-detector and in the limit perform as good as the AK-detector. We hereby emphasized that the requirement of having very high success rates, commonly needed for ambiguity-resolved parameter estimation, can be relaxed for detection, thus showing that improved model validation

is also possible with smaller ambiguity success rates. For the need of a case-by-case performance evaluation of the AR-detector, we also described the characteristics of its power function and provided a chi-square calculator-based simulation procedure for computing its probabilities.

5 Appendix

Proof of Lemma 2 We first derive the required expression for $\lambda_{\hat{e}} = ||P^{\perp}_{[A,B]}Cc||^2_{Q_{yy}}$. As (cf. 17)

$$[A, B] := \begin{bmatrix} 0 & G \\ L & G \end{bmatrix} \tag{44}$$

and L is invertible, a basis matrix of the orthogonal complement of $\mathcal{R}([A, B])$ is

$$[A, B]^{\perp} := \begin{bmatrix} G^{\perp} \\ 0 \end{bmatrix} \tag{45}$$

where $G^T Q^{-1}_{pp} G^{\perp} = 0$. We therefore have

$$P^{\perp}_{[A,B]} := \begin{bmatrix} P^{\perp}_G & 0 \\ 0 & 0 \end{bmatrix} \tag{46}$$

from which it follows that

$$\lambda_{\hat{e}} = ||P^{\perp}_{[A,B]}Cc||^2_{Q_{yy}} := ||P^{\perp}_G C_p c||^2_{Q_{pp}} \tag{47}$$

We now derive $\lambda_{\hat{\epsilon}(a)} = ||P_{\bar{A}}Cc||^2_{Q_{yy}}$. As the range space of $\bar{A}$ is orthogonal to that of $[B, [A, B]^{\perp}]$ and a basis matrix of the latter is

$$\begin{bmatrix} G & G^{\perp} \\ G & 0 \end{bmatrix} \tag{48}$$

, a basis matrix of the range space of $\bar{A}$ is

$$\bar{A} := \begin{bmatrix} G & 0 \\ -\epsilon G & G^{\perp} \end{bmatrix} \tag{49}$$

with $\epsilon = \sigma^2_{\phi}/\sigma^2_p$ (note: the above basis matrix should not be confused with the matrix $\bar{A}$ itself). Substitution of (49) into $P_{\bar{A}} = \bar{A}\bar{A}^{+}$ gives

$$P_{\bar{A}} := \begin{bmatrix} \frac{1}{1+\epsilon} P_G & -\frac{1}{1+\epsilon} P_G \\ -\frac{\epsilon}{1+\epsilon} P_G & P^{\perp}_G + \frac{\epsilon}{1+\epsilon} P_G \end{bmatrix} \tag{50}$$

from which it follows, with the assumed stochastic model of (17), that

$$\begin{aligned} \lambda_{\hat{\epsilon}(a)} &= ||P_{\bar{A}}Cc||^2_{Q_{yy}} \\ &:= ||P^{\perp}_G C_{\phi} c||^2_{Q_{\phi\phi}} + \frac{||P_G(C_p - C_{\phi})c||^2_{Q_{pp}}}{1+\sigma^2_{\phi}/\sigma^2_p} \end{aligned} \tag{51}$$

If we add this to $\lambda_{\hat{e}}$, we obtain the sought for expression for $\lambda_{\hat{e}(a)}$. □

Acknowledgements Chengyu Yin provided computational support and the figures, and both he and Christian Tiberius provided feedback and corrections to earlier versions of this contribution.

Data Availability All data generated or analysed during this study are included in this contribution.

Declarations

Conflict of interest The author declares that he has no conflict of interest to this work. We declare that we do not have any commercial or associative interest that represents a conflict of interest in connection with the work submitted.

References

DGCC (1982) The Delft approach for the design and computation of geodetic networks. "Forty years of thought" In: Anniversary edition on the occasion of the 65th birthday of Professor W Baarda By staff of the Delft Geodetic Computing Centre (DGCC) 1, pp 202–274

Duan B, Hugentobler U, Montenbruck O (2024) A method to assess the quality of GNSS satellite phase bias products. J Geod 28(2):89

Gillissen I, Elema I (1996) Test results of DIA: a real-time adaptive integrity monitoring procedure, used in an integrated navigation system. Int Hydrogr Rev 73(1):75–103

Koch KR (1987) Parameter estimation and hypothesis testing in linear models. Springer-Verlag Wien, New York

Lehmann R, Lösler M (2017) Congruence analysis of geodetic networks-hypothesis tests versus model selection by information criteria. J Appl Geod 11(4):271–283

Leick A, Rapoport L, Tatarnikov D (2015) GPS satellite surveying, 4th edn. John Wiley and Sons

Morio J, Balesdent M (2015) Estimation of rare event probabilities in complex aerospace and other systems: a practical approach. Woodhead Publishing, Sawston

Nowel K (2020) Specification of deformation congruence models using combinatorial iterative DIA testing procedure. J Geod 94(12):1–23

Perfetti N (2006) Detection of station coordinate discontinuities within the Italian GPS fiducial network. J Geod 80(7):381–396

Salzmann M (1993) Least squares filtering and testing for geodetic navigation applications. Netherlands geodetic commission, publications on geodesy, new series, no. 37

Strang G, Borre K (1997) Linear algebra, geodesy, and GPS. Wellesley-Cambridge Press

Teunissen PJG (2006) Testing theory: an introduction, 2nd edn. Delft University Press

Teunissen PJG, Montenbruck O (eds) (2017) Springer handbook of global navigation satellite systems. Springer

Teunissen PJG, Verhagen AA (2023) PDF evaluation of elliptically contoured GNSS integer ambiguity residuals. X Hotine-Marussi symposium on mathematical geodesy, international association of geodesy symposia, pp 1–7

Teunissen PJ, Kleusberg A (eds) (1998) GPS for geodesy, 2nd Edition. Springer-Verlag

Teunissen PJG (1995) The least squares ambiguity decorrelation adjustment: a method for fast GPS integer estimation. J Geod 70:65–82

Teunissen PJG (1997) A canonical theory for short GPS baselines. Part IV: precision versus reliability. J Geod 71:513–525

Teunissen PJG (1999) An optimality property of the integer least-squares estimator. J Geod 73:587–593

Teunissen PJG (1999) The probability distribution of the GPS baseline for a class of integer ambiguity estimators. J Geod 73(5):275–284

Teunissen PJG (2000) Probabilistic Properties of GNSS Integer Ambiguity Estimation. Earth Planets Space 52:801–805

Teunissen PJG (2002) The parameter distributions of the integer GPS model. J Geod 76:41–48

Teunissen PJG, Salzmann MA (1989) A recursive slippage test for use in state-space filtering. Manuscr Geod 14:383–390

Yang L, Shen Y, Li B, Rizos C (2021) Simplified algebraic estimation for the quality control of DIA estimator. J Geod 95:1–15

Yu Y, Yang L, Shen Y, Sun N (2023) A DIA method based on maximum a posteriori estimate for multiple outliers. GPS Solut 27(4):199